 https://doi.org/10.3311/PPci.37258

Periodica Polytechnica Civil Engineering, 69(1), pp. 136–145, 2025

Optimization of Load-transfer Functions for a Large-diameter Pile in Multi-layered Geological Conditions *via* a Stochastic Search Algorithm

Juraj Chalmovský[1*]

[1] Department of Geotechnics, Faculty of Civil Engineering, Brno University of Technology, Veveri 331/95, 60200 Brno, Czech Republic
[*] Corresponding author, e-mail: chalmovsky.j@fce.vutbr.cz

Received: 04 May 2024, Accepted: 24 September 2024, Published online: 09 October 2024

Abstract

The paper presents the combination of the load transfer method (computational model) and the genetic algorithm (optimization model) for the automated inverse analysis of instrumented pile load tests. The output of this process are the input parameters governing the shape of the load-transfer functions and thus the prediction accuracy when the load-transfer method is used as a design tool for deep foundations. The optimization problem is converted into an unconstrained task by applying the static penalty approach. Two types of measurements are considered in a newly proposed objective function: the load-displacement curve monitored in a pile head and the axial force profiles along a pile derived from strain gauges. Firstly, the local sensitivity analysis via the Design of Experiments is carried out to identify the parameters of the genetic algorithm which significantly influences the rate of convergence during the optimization process. Subsequently, a fully automated inverse analysis of the loading test of the large-diameter bored pile in multilayered geological conditions is presented. The simultaneous combination of two instrumentation sources leads to a stable unique solution with a sufficient match between the prediction and measurements despite a larger number of unknown – optimized variables.

Keywords

load-transfer method, genetic algorithm, optimization, load-displacement curve, large-diameter pile

1 Introduction

The load-transfer (t-z) method is a well-established design tool in geotechnical engineering. To determine the values of input parameters governing the shape of load transfer curves, it is appropriate to perform the back analysis of an instrumented loading test. However, the performance of such an analysis via a trial-error procedure can be time-consuming due to the following reasons: multilayered geological conditions, the application of a load-transfer function defined by multiple parameters, or the need to conduct a back analysis on a larger number of loading tests.

The proposed paper presents a combination of the load transfer method for large-diameter piles with the stochastic optimization model in order to automate and thus increase the time and cost-efficiency of the back-analysis process.

First, a sensitivity study of the parameters governing the optimization model via the Design of Experiments (DOE) was conducted. Subsequently, the automated back analysis of a large-diameter pile load test was performed.

2 Load-transfer method

Introduced by Seed and Reese [1], the load-transfer method has become an accepted computational method. It was initially used for the prediction of the load-displacement response of large-diameter axially loaded tension piles [2–4] and others and compression piles [5, 6] and others. Several modifications and improvements to the original procedure were derived for various types of geotechnical constructions, such as piles subjected to loading-unloading cycles [7], rectangular closed diaphragm walls [8], and pile groups [9]. A similar technique called the p-y method is also available for horizontally loaded piles [10]. The axial load-transfer method (t-z method) is based on the idea that an axially loaded member (e.g., a tension or compression pile) can be divided into a finite number of segments which are each assigned a unique dependence between the segment's vertical displacement (s_s) and the shear stress mobilized on its surface (q_s). The function is called the load-transfer (mobilization) function (curve). A similar

Cite this article as: Chalmovský, J. "Optimization of Load-transfer Functions for a Large-diameter Pile in Multi-layered Geological Conditions *via* a Stochastic Search Algorithm", Periodica Polytechnica Civil Engineering, 69(1), pp. 136–145, 2025. https://doi.org/10.3311/PPci.37258

function between the normal stress at the pile base (q_b) and the corresponding base displacement (s_b) is added for the pile tip in the case of compressive loads. Load-transfer functions are in general represented by nonlinear springs that replace both the pile-soil interface and the soil continuum (Fig. 1). Various load-transfer curves are available in the literature and can be categorized as follows:

1. Linear elastic – perfectly plastic functions [11, 12];
2. Bilinear, trilinear curves [13, 14];
3. Nonlinear – hyperbolic and cubic root curves [15, 16].

The hyperbolic load-transfer function for the shaft (Eq. (1)) and the base (Eq. (2)) proposed by [15] were adopted in this study, where $q_{s,ult}$ is the ultimate skin friction, $q_{b,ult}$ is the ultimate base resistance, B is the pile diameter, and M_s and M_b are the stiffness parameters governing the initial slope of the load-transfer functions of the shaft and base, respectively:

$$q_s = \frac{q_{s,ult} s_s}{M_s B + s_s}, \tag{1}$$

$$q_b = \frac{q_{b,ult} s_b}{M_b}. \tag{2}$$

3 Stochastic optimization methods

Stochastic optimization methods have become increasingly popular in the geotechnical engineering during the recent decades. Several algorithms belong to this category, the basic ones are listed below:

- particle swarm optimization (PSO) [17];
- genetic algorithms (GA) [18];
- differential evolution algorithm (DE) [19];
- artificial bee colony (ABC) [20];
- ant colony optimization (ACO) [21].

The application of these methods and their modifications might be divided into two main areas of the geotechnical engineering:

- Inverse modelling and soil parameter identification especially for complex soil constitutive models (f. e. [22, 23]).
- Structural optimizations (f. e. [24, 25]) which might be further divided into the topology optimization, shape optimization and dimensional optimization.

Further evolution of the single objective optimization procedures (SOOP) led to the development of the multiple optimization techniques (MOOP), in which multiple objective functions are considered simultaneously. Comprehensive overview of MOOPs might be found in [26] and [27]. 5 different MOOPs were compared for the time-continuous optimization-based updating of predictions during the deep excavation project in the latter one.

The development of the stochastic optimization methods was based on the laws of natural genetics and the natural selection and motivated by the several limitations of commonly used search procedures such as the gradient-based methods. The main limitations of these classical methods can be summarized as follows [28]:

- The convergence depends on the initial solution and is sensitive to the presence of local optimums.
- The partial derivates of the objective function must be evaluated (the objective function must be known a priori).
- Parallel computing cannot be utilized effectively.

GAs provides a significantly different approach compared to the classical optimization techniques. The flowchart of a basic GA is shown in Fig. 2. First, the solution (the values of the input parameters of the load transfer functions in the current case) is binary coded. Each binary string (chromosome) consists of a predefined number of bits (genes). The length of the chromosome (the number of genes) depends on the number of input parameters and the required number of levels of each parameter. For example, two input parameters are needed for analysis of a pile

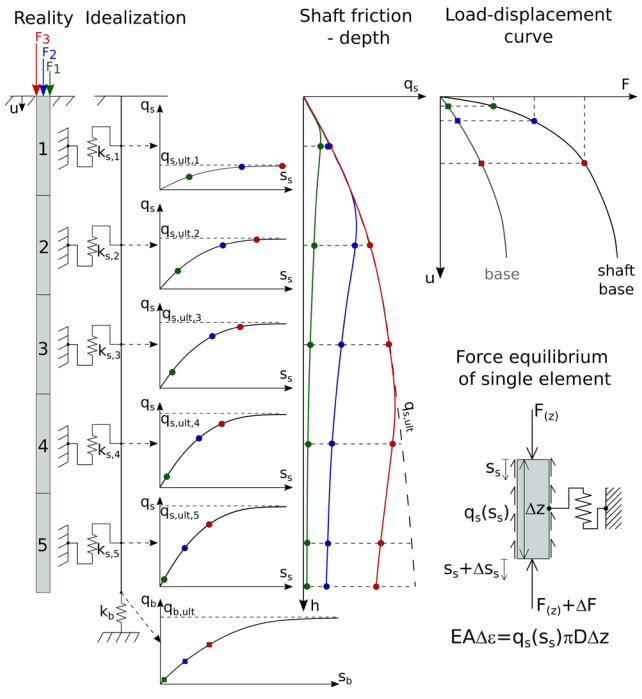

Fig. 1 Discretization of an axially loaded member into the predefined number of elements and assignment of load-transfer functions

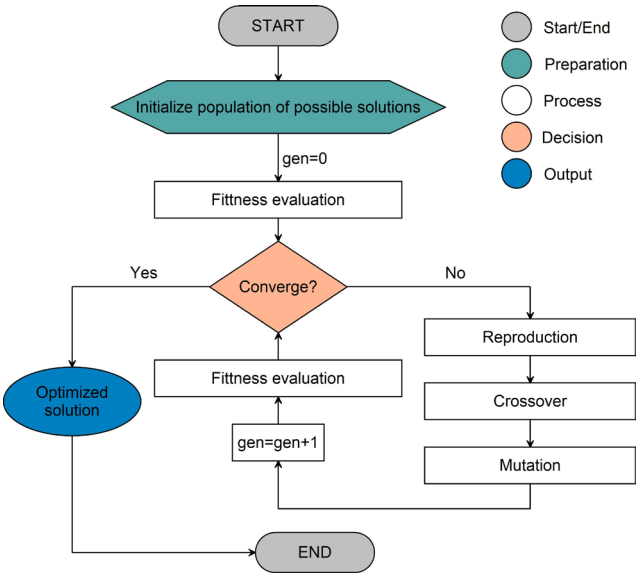

Fig. 2 Flowchart of a GA

loaded by tension and situated in a single geological layer via the load-transfer method: the ultimate shaft friction $q_{s,ult}$ and the shaft stiffness parameter M_s. The length of the part of the chromosome l_i belonging to each input parameter is given by Eq. (3), where n_{alt} is the required number of levels of the given parameter. 64 levels of two parameters therefore require a binary string consisting of 12 bits:

$$n_{alt} = 2^{l_i}. \tag{3}$$

To use non-integer values of input parameters, the following mapping rule is utilized:

$$x_i = x_i^{\min} + \frac{x_i^{\max} - x_i^{\min}}{2^{l_i}} DV(s_i), \tag{4}$$

where x_i is the current (non-integer) value of the input parameter, $x_i^{\min}$ and $x_i^{\max}$ are the lower and upper limits, respectively, $DV(s_i)$ is the decoded (integer) value of the given input parameter.

The first population of possible solutions (members) is randomly generated during the initialization. The fitness (objective function value) of each member is evaluated.

A specific formulation of the objective function considering both the measured load-displacement curve in the pile head and the axial strain profiles along the pile is proposed in Section 5. The primary objective of the reproduction operator is to increase the number of members with above-average fitness values. The binary tournament selection operator was used for this purpose. The crossover and mutation operators manipulate the binary coding of the chosen members and thus create new solutions and maintain their diversity. The single-point crossover operator (Fig. 3) is adopted in this study. Two solutions are selected

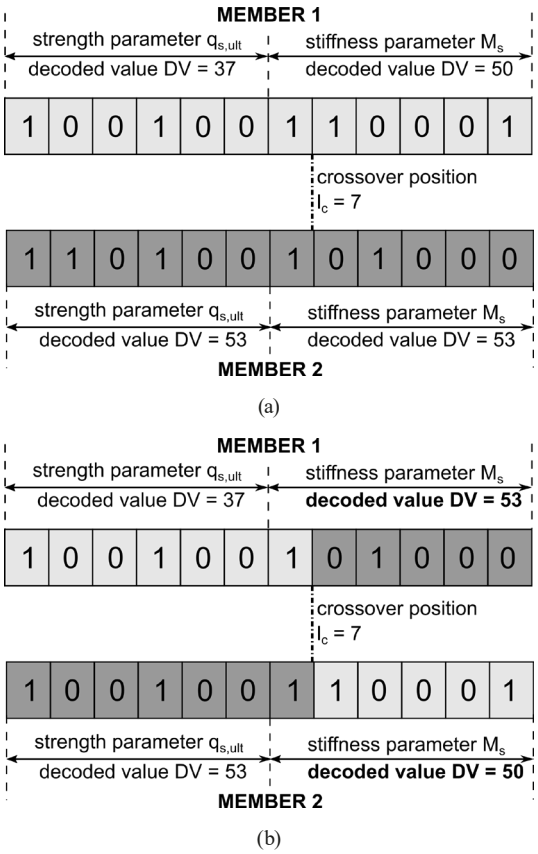

Fig. 3 Principle of crossover operator; (a) Binary strings of two members before crossover; (b) Binary strings of two members after crossover

and a single cross-site (position in the binary string l_c) is chosen randomly. The segments of binaries to the right of the cross-site are exchanged with each other. The number of solutions used in the crossover is governed by the crossover probability p_c. The mutation operator changes the value of only one bit (gene) at a position l_m with a small mutation probability p_m (Fig. 4). At this point a new generation of solutions is completed, the fitness value of each one is evaluated and the whole process is repeated until a prescribed value of the objective function is reached.

The theoretical concept of GAs is based on the Schema Theorem [18]. A schema is a sequence of bits which repeats itself in binary strings of solutions across generations. If a particular schema produces a solution with the above average fitness, the number of this schema increases. According to the Schema Theorem, the number of schema H at time $t + 1$ is given as:

$$m(H,t+1) \geq m(H,t)\frac{f(H)}{\bar{f}}\left[1 - p_c\frac{\delta(H)}{l-1} - o(H)p_m\right], \tag{5}$$

where $m(H, t + 1)$ and $m(H, t)$ are the number of the schema H at time t and $t + 1$, respectively, $f(H)$ is the

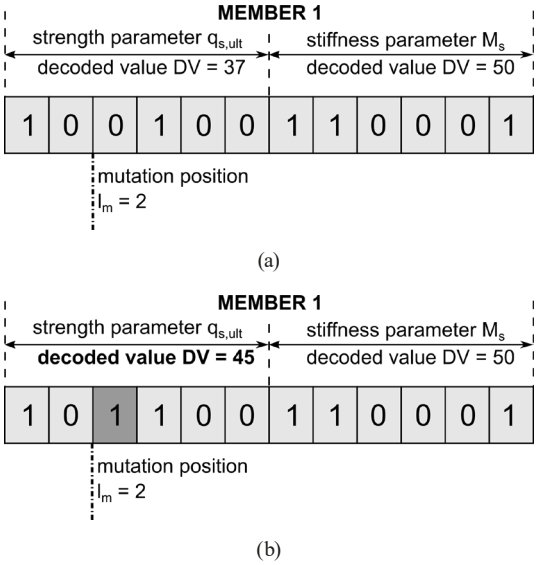

Fig. 4 Principle of mutation operator; (a) Binary string of one member before mutation; (b) Binary string of one member after mutation

fitness of a particular schema H, $\bar{f}$ is the average fitness, p_c is the cross-over probability, p_m is the mutation probability, l is the length of H, and $\delta(H)$ and $o(H)$ are the length and the order of schema H, respectively.

4 Analyzed pile load test

The large-scale pile load test was conducted in the city of Brno in the Czech Republic [29]. The cover of the tertiary deposits in the particular area consists of Quaternary fluvial sediments of sandy clay (saCl), with a sand fraction of up to 30%. The thickness of these sediments ranges from 4 to 6 m. The pre-Quaternary base is formed from clay (Cl) with the gradually increasing consistency from soft to stiff.

The tested bored pile was 880 mm in diameter and 16 m long. The first meter of the pile was equipped with an outer steel ring which separated the pile from the surrounding soil. The pile is therefore considered to be 15 m long in the presented analysis. The load test was monitored in a standard manner, which involved the measurement of loads and displacements in the pile head. The pile was additionally equipped with 10 vibrating wire tensometers placed at 5 different depths: 1.0 m; 4.5 m; 8.0 m; 11.5 m and 15.0 m (Fig. 5).

The test procedure consisted of 13 loading stages, including 2 unloading – reloading cycles. The load at a given load stage was held constant until the acceptance criterion was fulfilled. The measured load-displacement curve and axial load distributions are shown in Figs. 6 and 7, respectively.

The load level of 2000 kN was the last one at which the acceptance criterion was fulfilled. Pile settlement

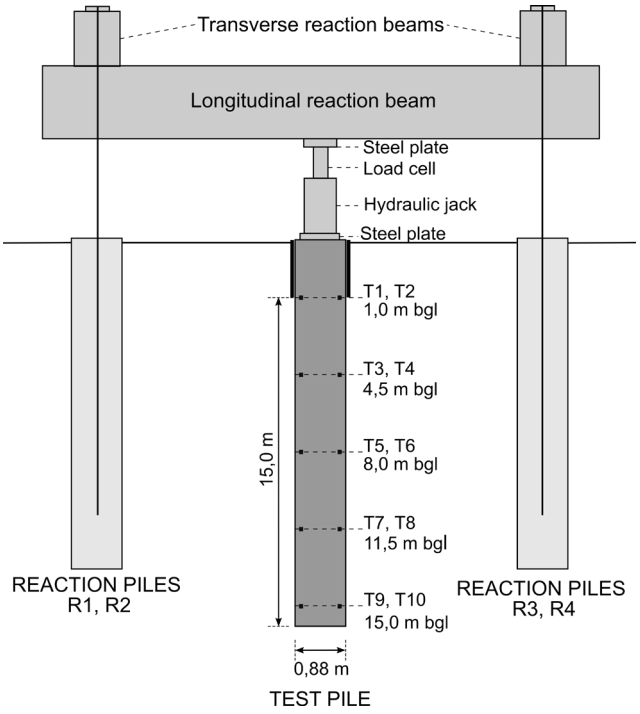

Fig. 5 Setup of analyzed static load test

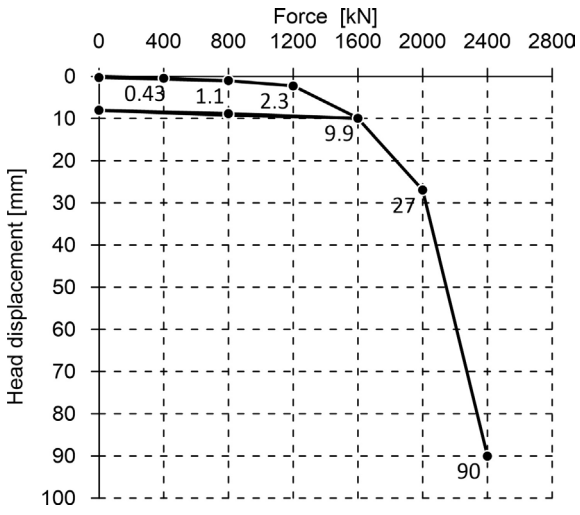

Fig. 6 Measured load – displacement curve

started to increase rapidly during the subsequent loading. The load level of 2400 kN was reached; however, no settlement stabilization occurred, and the test was ended. The axial load profiles derived from the strain measurements revealed three distinct sections with the substantially different ultimate skin frictions. These sections are considered as three independent soil layers with the thicknesses of 3.5; 3.5 and 8 meters. It is interesting to note that the sudden change in the slope of the axial force profiles at a depth of 3.5 m approximately coincides with the position of the interface between the Quaternary (sandy clays) and the pre-Quaternary deposits (clays). The vector of the

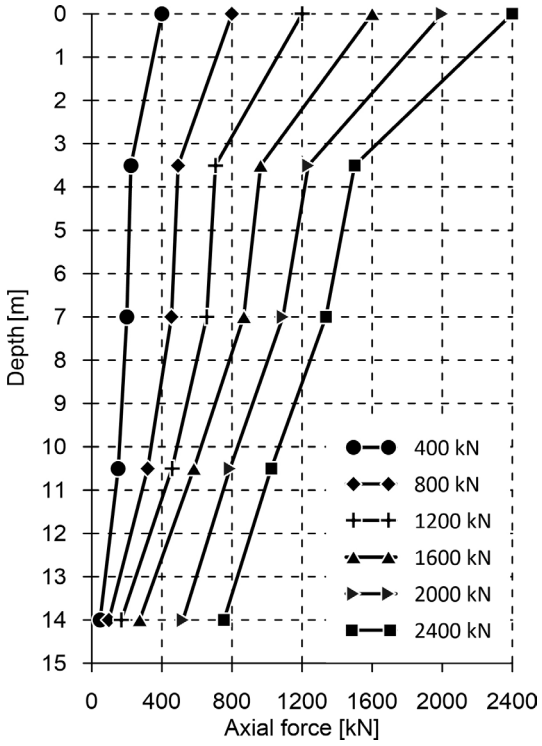

Fig. 7 Measured axial force profiles

optimized (unknown) variables X (Eq. (6)) governing the shape of the load transfer functions has 8 members: 6 for the shaft and 2 for the pile base.

$$X = \left(q_{s,ult}^{1}, M_{s}^{1}, q_{s,ult}^{2}, M_{s}^{2}, q_{s,ult}^{3}, M_{s}^{3}, q_{b,ult}, M_{b}\right) \tag{6}$$

5 Formulation of the optimization task

The optimization task presented in this paper is considered as a constrained minimization problem which is further converted into an unconstrained one by applying the static penalty approach [30]. The expanded objective function $\varnothing(X)$ is defined as:

$$\varnothing(X) = f(X) + p(X), \tag{7}$$

where $f(X)$ is the fitness function quantifying the differences between the measurements and predictions and $p(X)$ is the penalty function. The fitness function was formulated using the weighted sum method and consists of two components (Eq. (8)): the differences between the measured and predicted load-displacement curves and the axial strain (force) profiles are quantified via the load-displacement term ($f_{ld}(X)$) and the strain term ($f_{str}(X)$), respectively. Their relative contributions to the overall value of the fitness function $f(X)$ are governed by the weight factors k_{ld} and k_{str}.

$$f(X) = k_{ld} f_{ld}(X) + k_{str} f_{str}(X) \tag{8}$$

Both the displacements and respective forces should be considered in the load-displacement term. Thus, the approximate residual area $A_{res}(X)$ between the computed and the measured load-displacement curve is determined via the trapezoidal rule (Eq. (9)). $F_{p,i}$ and $F_{m,i}$ are the predicted and measured pile head loads, respectively. $u_{p,i}$ and $u_{m,i}$ are the corresponding pile head movements and n is the total number of computational steps. $A_{res}(X)$ is normalized by the area below the predicted load-displacement curve $A_p(X)$ (Eq. (10)).

$$A_{res}(X) = \sum_{i=1}^{n} \frac{u_{p,i} - u_{p,i-1}}{2} \begin{bmatrix} \left(F_{p,i} - F_{m,i}\right) \\ +\left(F_{p,i-1} - F_{m,i-1}\right) \end{bmatrix} \tag{9}$$

$$f_{ld}(X) = \frac{A_{res}(X)}{A_p(X)} \tag{10}$$

The second term of the fitness function ($f_{str}(X)$) for a particular loading stage is formulated as the average relative difference between the measured and predicted axial forces from all positions of the strain gauges (Eq. (11)). $T_{p,j}$ and $T_{m,j}$ are the calculated and measured axial forces, respectively, and n_{str} is the number of strain gauges along the pile.

$$f_{str}(X) = \frac{1}{n_{str}} \sum_{j=1}^{n_{str}} \frac{T_{p,j} - T_{m,j}}{T_{p,j}} \tag{11}$$

The penalty function $p(X)$ is defined as:

$$p(X) = \begin{cases} 0 & F_{p,ult} < F_{m,ult} \\ R_k \max\left[0, g(X)\right]^2 & F_{p,ult} \geq F_{m,ult} \end{cases}, \tag{12}$$

while $g(X)$ is the constrained function (Eq. (13)) and R_k is the penalty coefficient (Eq. (14)). $F_{m,ult}$ and $F_{p,ult}$ are the measured and predicted ultimate forces, respectively. $g(X)$ depends on the $F_{m,ult} / F_{p,ult}$ ratio similarly to the fitness function $f(X)$. Adding the constrained function to the objective function (Eq. (7)) ensures that solutions with the predicted ultimate bearing capacity higher than the measured one will be penalized. The descent factor n_s in Eq. (14) controls the rate of increase in the penalty function as the difference between the measured and predicted bearing capacity increases. The impact of the descent factor n_s on the expanded objective function shape is illustrated in Fig. 8.

The penalty function is formulated in such a way that slightly infeasible solutions have sufficiently low penalties and thus the exploration of a slightly infeasible region by the GA is not prevented. In other words, an infeasible solution with a predicted ultimate capacity that is 5% above

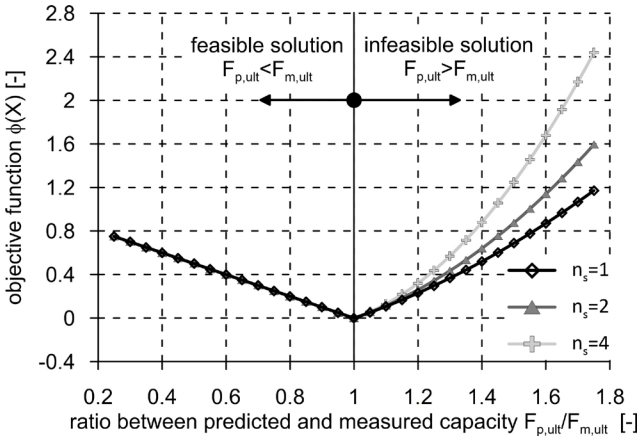

Fig. 8 Expanded objective functions for different descent factor values

a measured capacity will probably be closer to an optimal solution than one that yields a feasible prediction of the ultimate bearing capacity that is 50% below the measured one.

$$g(X)=\frac{F_{p,ult}(X)}{F_{m,ult}}-1 \tag{13}$$

$$R_k = n_s \max\left(f(X)\right) \tag{14}$$

6 Sensitivity analysis of GA settings

The GA's search process is controlled by 8 parameters:

- n_{gen}: number of generations (iterations);
- n_{alt}: number of levels of each optimized variable;
- n_{pop}: number of members in populations, each member is represented by an individual set of values of input parameters;
- p_c: crossover probability;
- p_m: mutation probability;
- n_s: descent factor;
- k_{ld}, k_{str}: weight factors.

In order to set these parameters appropriately, local sensitivity analysis was performed via the Design of Experiment (DOE). Both the load transfer method and the genetic algorithm were programmed in the form of scripts in the Python programming language. All parameters except the mutation probability (p_m) and the weight factor for the strain measurements (k_{str}) were involved in the sensitivity analysis. The upper and lower bounds of the analyzed parameters are summarized in Table 1. The mutation probability p_m is much lower than the crossover probability p_c and thus a lower impact on the optimization process might be expected. The weight factor of the strain measurements is not an independent variable as the sum of both factors (k_{ld}, k_{str}) is equal to one.

Table 1 List of variables involved in the sensitivity analysis

Variable	Lower bound (LB)	Upper bound (UB)
n_{gen}	15	60
n_{alt}	128	512
n_{pop}	32	128
p_c	0.5	0.9
n_s	2	4
k_{ld}	0.2	0.8

A full factorial design with two levels of each factor (2^k) and three repetitions of the design of experiments was implemented. Thus, a total of 192 optimization runs were required. The mean of the objective function $\overline{\varnothing(X)}$ (Eq. (15)) after reaching the final generation was chosen as the output variable for the subsequent statistical evaluation. A Pareto chart of the standardized effects is shown in Fig. 9.

$$\overline{\varnothing(X)}=\frac{\sum_{i=1}^{n_{pop}}\varnothing(X_i)}{n_{pop}} \tag{15}$$

Based on the t-test with the null hypothesis that the effect of the particular parameter is zero on the significance level of 0.05 and considering only primary effects, it might be concluded that factors n_{gen}, n_{alt}, p_c and k_{ld} have significant effects on the efficiency of the optimization process. The primary effects of these terms are summarized in Table 2.

Increasing the number of generations n_{gen} led to a significant decrease in the $\overline{\varnothing(X)}$ value. The trend is opposite for the crossover probability p_c. Increasing this probability caused the generation of too many new original members in the subsequent iteration and thus slowed the process of reduction of the objective function. It seems that relying solely on the results of standard monitoring (the load-displacement curve in the pile head) by increasing the k_{ld} value resulted in a higher $\overline{\varnothing(X)}$ value. It is

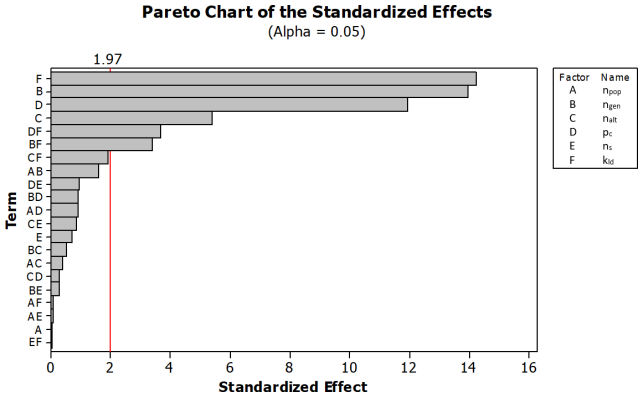

Fig. 9 Pareto chart of the standardized effects

Table 2 Estimated primary effects of statistically significant terms

Variable	n_{gen}	n_{alt}	p_c	k_{ld}
Effect	−0.03925	−0.01515	0.03356	0.03994

Effect plot

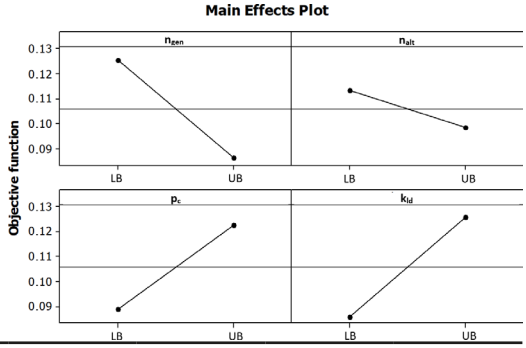

therefore important to combine at least two sources of measurements in similar applications.

Increasing the descent factor n_s resulted in a small drop in the objective function compared to the previously mentioned factors. It is also interesting to note that, within the chosen limits, the size of the population n_{pop} is significantly less important than the number of levels of each variable n_{alt}. It seems that the crossover and mutation operators are able to create enough new and possibly better solutions throughout the optimization process regardless of the initial population size.

7 Case study – pile load test in multi-layered geological conditions

Based on the results of the sensitivity study, the following GA settings were applied in the case study: n_{gen} = 45, n_{alt} = 256, n_{pop} = 64, p_c = 0.5, p_m = 0.05, n_s = 2, k_{ld} = 0.2, k_{str} = 0.8. The optimized values of each input variable are summarized in Table 3. The ultimate skin frictions correspond to the distributions of axial forces along the pile. The highest ultimate shaft friction value predicted in the 1st layer might be due to the significant amount of sand fraction present in this stratum. The presence of the second (weak) layer is considered correctly as the lowest ultimate skin friction value and the highest value of M_s (indirectly proportional to the initial stiffness of the load-transfer curve) was identified in this layer. The values obtained for the stiffness parameters are within the range recommended by [15]: the average value of M_s = 0.0038 and M_b = 0.01. Fig. 10 illustrates the gradual convergence of the predicted load-displacement curves towards the measured curve. For the purpose of clarity, only the predictions in four selected generations (1, 5, 15, 30) and for the first 20 members are shown here. It is obvious from this image that the load-displacement curves obtained from randomly generated inputs gradually converge towards a unique solution that is close to the measured load-displacement curve.

Table 3 Selected ranges and final (optimal) values of parameters controlling the shape of load-transfer functions

Group	X_i	Unit	$X_{i,\min}$	$X_{i,\max}$	$X_{i,opt}$
Shaft stiffness	M_s^1	–	0.0013	0.0076	0.0055
	M_s^2	–	0.0013	0.0076	0.0061
	M_s^3	–	0.0013	0.0076	0.0043
Shaft strength	$q_{s,ult}^1$	kPa	10	100	82.1
	$q_{s,ult}^2$	kPa	10	50	11.4
	$q_{s,ult}^3$	kPa	10	100	41.3
Base stiffness	M_b	–	0.005	0.03	0.024
Base strength	$q_{b,ult}$	kPa	750	2000	948.4

The shape of the expanded objective function, its load-displacement term ($f_{ld}(X)$) and the strain term ($f_{str}(X)$) are shown in Fig. 11. No significant reduction in the objective function value was observed after the 30th generation. Similar plots are shown for $q_{s,ult}$, $q_{b,ult}$ and M_s, M_b in Figs. 12 and 13, respectively. These are the average values of the corresponding parameter in each generation.

The ultimate skin frictions and the tip resistance reach stable values between the 16th and 18th generation, which is earlier than the corresponding stiffness parameters.

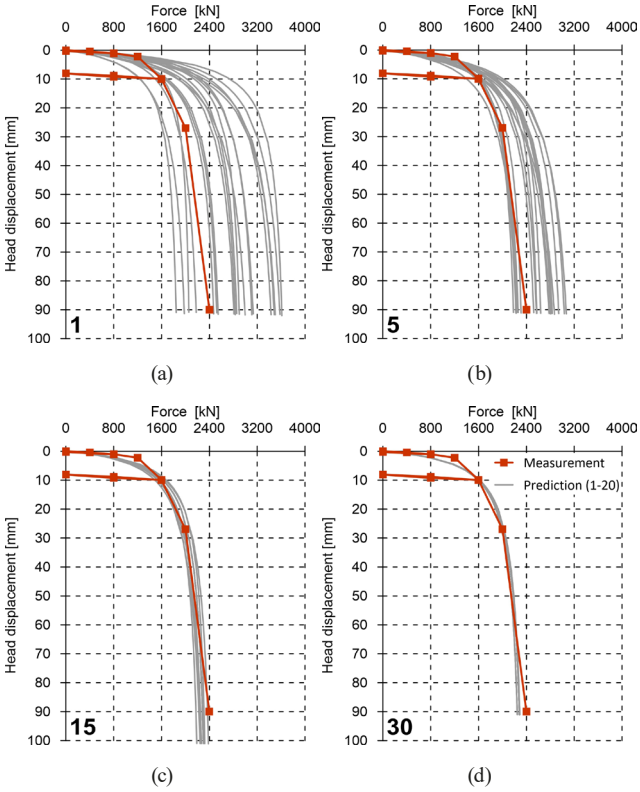

Fig. 10 Predicted load-displacement curves for 20 members in four different generations (1, 5, 15 and 30); (a) Generation no. 1; (b) Generation no. 5; (c) Generation no. 15; (d) Generation no. 20

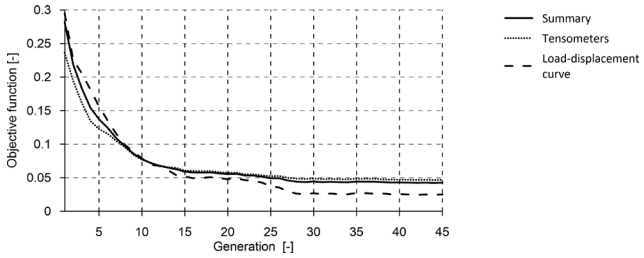

Fig. 11 The progression of the objective function during optimization

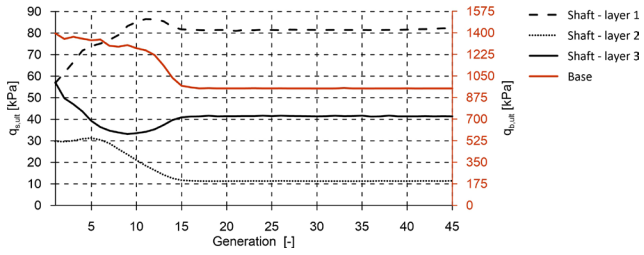

Fig. 12 The progression of the $q_{s,ult}$ and $q_{b,ult}$ parameters during optimization

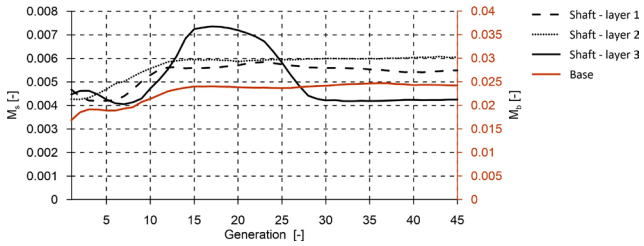

Fig. 13 The progression of the M_s and M_b parameters during optimization

The average value of the tip resistance in the first iteration (both generated randomly) is overestimated and the GA algorithm significantly upgrades this value throughout the optimization process.

The optimized prediction and measured axial force profiles are compared in Fig. 14. The predicted force profile for the last load level (2400 kN) is not shown here as the computed ultimate bearing capacity was lower than the measured one. The GA search algorithm was able to distinguish between three layers, although it slightly underestimates the skin friction in the first layer. Very low and moderate skin frictions in the second and third layers, respectively, are predicted with a good accuracy.

8 Conclusions

The combination of the axial load-transfer method for the compression piles (the computational model) and the genetic algorithm (the optimization model) was presented in this paper. In this way, it is possible to automate inverse analysis of instrumented loading tests and thus decrease the time and financial requirements of the back-analysis process. This process can be useful especially in situations where many tests need to be analyzed.

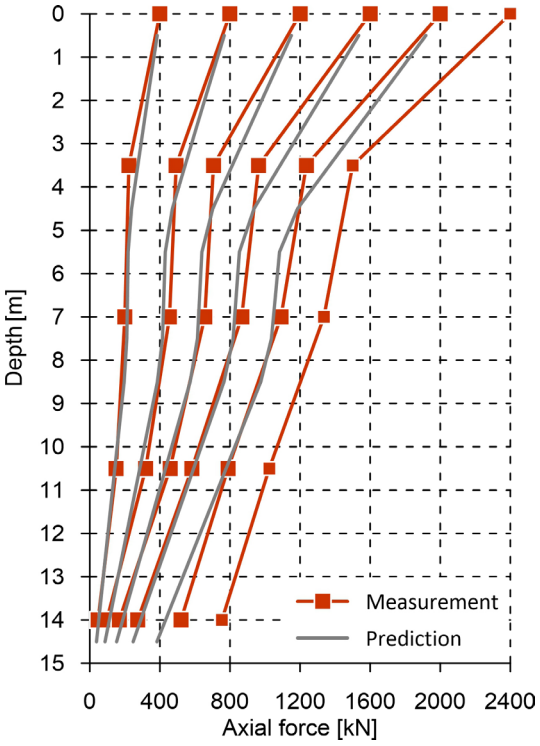

Fig. 14 Measured axial force profiles and their optimized predictions

The modified penalty approach was utilized in order to transform the constrained optimization task into the unconstrained one. Predictions with a higher-then-measured ultimate bearing capacity were penalized. Two sources of measurements were combined into the objective function: the load-displacement response in the pile head and the axial load profiles along the pile for different loading stages. Sensitivity analysis revealed that increasing the number of generations and the number of levels of input variables improves the prediction accuracy. In contrast, increasing the crossover probability too much leads to a slower convergence rate as many new and possibly low-fitness solutions are created in subsequent generations.

The case study of the loading test of the large-diameter bored pile demonstrated that predictions obtained from inputs generated randomly in the first iteration converged towards a unique solution that was in acceptable agreement with the both sources of measurements. Two types of measurements recorded throughout the test (the load-displacement curve in the pile head and the axial force profiles along the pile) proved to be an important factor as the values of 8 input parameters were searched for.

Acknowledgement

The research was supported by the Technology Agency of the Czech Republic under project no. ZETA2-TJ02000140.

References

[1] Seed, H. B., Reese, L. C. "The Action of Soft Clay along Friction Piles", Transactions of the American Society of Civil Engineers, 122(1), pp. 731–754, 1957. https://doi.org/10.1061/TACEAT.0007501

[2] Reddy, E. S. B., O'Reilly, M., Chapman, D. "A software to predict the behavior of tension piles", Computers & Structures, 62(4), pp. 653–658, 1997. https://doi.org/10.1016/S0045-7949(97)80002-3

[3] Reddy, E. S. B., O'Reilly, M., Chapman, D. N. "Modified T-Z model—a software for tension piles", Computers and Structures, 68(6), pp. 613–625, 1998. https://doi.org/10.1016/S0045-7949(98)00089-3

[4] Sulaiman, I. H., Coyle, H. M. "Uplift Resistance of Piles in Sand", Journal of the Geotechnical Engineering Division, 102(5), pp. 559–562, 1976. https://doi.org/10.1061/AJGEB6.0000275

[5] Boonyatee, T., Lai, Q. V. "A non-linear load transfer method for determining the settlement of piles under vertical loading", International Journal of Geotechnical Engineering, 14(2), pp. 206–217, 2020. https://doi.org/10.1080/19386362.2017.1410337

[6] Zhang, Q., Zhang, Z. "A simplified nonlinear approach for single pile settlement analysis", Canadian Geotechnical Journal, 49(11), pp. 1256–1266, 2012. https://doi.org/10.1139/t11-110

[7] Dias, T. G. S., Bezuijen, A. "Load-Transfer Method for Piles under Axial Loading and Unloading", Journal of Geotechnical and Geoenvironmental Engineering, 144(1), 04017096, 2018. https://doi.org/10.1061/(ASCE)GT.1943-5606.0001808

[8] Wu, J., Cheng, Q., Wen, H., Wang, L., Li, Y., Zhang, J. "A load transfer approach to rectangular closed diaphragm walls", Proceedings of the Institution of Civil Engineers - Geotechnical Engineering, 169(6), pp. 509–526, 2016. https://doi.org/10.1680/jgeen.15.00156

[9] Zhang, Q., Li, S., Liang, F., Yang, M., Zhang, Q. "Simplified method for settlement prediction of single pile and pile group using a hyperbolic model", International Journal of Civil Engineering, 12(2), pp. 146–159, 2014.

[10] Reese L. C., Van Impe, W. F. "Single Piles and Pile Groups Under Lateral Loading", Taylor & Francis, 2011. ISBN 9780415469883

[11] Randolph, M. F., Wroth, C. P. "Analysis of Deformation of Vertically Loaded Piles", Journal of the Geotechnical Engineering Division, 104(12), pp. 1465–1488, 1978. https://doi.org/10.1061/AJGEB6.0000729

[12] Verbrugge, J.C. "Évaluation du tassement des pieux à partir de l'essai de pénétration statique" (Evaluation of pile settlement using cone penetrometre test), Revue Française de Géotechnique, 15, pp. 75–82, 1981. (in French) https://doi.org/10.1051/geotech/1981015075

[13] Frank, R., Zhao, S. R. "Estimation par les paramètres pressiométriques de l'enfoncement sous charge axiale de pieux forés dans des sols fins" (Estimation by pressuremeter parameters of the penetration under axial load of bored piles in fine soils), Bulletin de Liaison des Laboratoires des Ponts et Chaussées, 119, pp. 17–24, 1982. (in French)

[14] Frank, R. "Recent developments in the prediction of pile behaviour from pressuremeter tests", Building Science, 2, pp. 14–24, 1988.

[15] Bohn, C., Lopes dos Santos, A., Frank, R. "Development of Axial pile Load Transfer Curves Based on Instrumented Load Tests", Journal of Geotechnical and Geoenvironmental Engineering, 143(1), 04016081, 2017. https://doi.org/10.1061/(ASCE)GT.1943-5606.0001579

[16] Fleming, W. G. K. "A new method for single pile settlement prediction and analysis", Géotechnique, 42(3), pp. 411–425, 1992. https://doi.org/10.1680/geot.1992.42.3.411

[17] Eberhart, R., Kennedy, J. "A new optimizer using particle swarm theory", In: MHS '95. Proceedings of the Sixth International Symposium on Micro Machine and Human Science, Nagoya, Japan, 1995, pp. 39–43. ISBN 0-7803-2676-8 https://doi.org/10.1109/MHS.1995.494215

[18] Goldberg, D. E. "Genetic Algorithms in Search, Optimization & Machine Learning", Addison-Wesley Publishing Company, Inc., 1989. ISBN 0-201-15767-5

[19] Karaboga, D. "An idea based on honey bee swarm for numerical optimization", Erciyes University, Kayseri, Türkiye, Rep. TR06, 2005.

[20] Storn, R., Price, K. "Differential Evolution – A Simple and Efficient Heuristic for Global Optimization over Continuous Spaces", Journal of Global Optimization, 11(4), pp. 341–359, 1997. https://doi.org/10.1023/A:1008202821328

[21] Dorigo, M., Di Caro, G. "Ant colony optimization: a new meta-heuristic", In: Proceedings of the 1999 Congress on Evolutionary Computation-CEC99 (Cat. No. 99TH8406), Washington, DC, USA, 1999, pp. 1470–1477. ISBN 0-7803-5536-9 https://doi.org/10.1109/CEC.1999.782657

[22] Meier, J., Schaedler, W., Borgatti, L., Corsini, A., Schanz, T. "Inverse Parameter Identification Technique Using PSO Algorithm Applied to Geotechnical Modelling", Journal of Artificial Evolution and Applications, 2008(1), 574613, 2008. https://doi.org/10.1155/2008/574613

[23] Yin, Z.-Y., Jin, Y.-F., Shen, J. S., Hicher, P.-Y. "Optimization techniques for identifying soil parameters in geotechnical engineering: Comparative study and enhancement", International Journal for Numerical and Analytical Methods in Geomechanics, 42(1), pp. 70–94, 2018. https://doi.org/10.1002/nag.2714

[24] Pucker, T., Grabe, J. "Structural optimization in geotechnical engineering: basics and application", Acta Geotechnica, 6(1), pp. 41–49, 2011. https://doi.org/10.1007/s11440-011-0134-7

[25] Seitz, K.-F., Grabe, J. "Three-dimensional topology optimization for geotechnical foundations in granular soil", Computers and Geotechnics, 80, pp. 41–48, 2016. https://doi.org/10.1016/j.compgeo.2016.06.012

[26] Panagant, N., Kumar, S., Tejani, G. G., Pholdee, N., Bureerat, S. "Manyobjective meta-heuristic methods for solving constrained truss optimisation problems: A comparative analysis", MethodsX, 10, 102181, 2023. https://doi.org/10.1016/j.mex.2023.102181

[27] Yin, Z.-Y., Jin, Y.-F. "Practice of Optimisation Theory in Geotechnical Engineering", Springer Singapore, 2019. ISBN 978-981-13-3408-5 https://doi.org/10.1007/978-981-13-3408-5

[28] Deb, K. "An introduction to genetic algorithms", Sadhana, 24(4), pp. 293–315, 1999. https://doi.org/10.1007/BF02823145

[29] Misove, P., Velic, P. "Zpráva Zatěžovací zkouška piloty – Brno, MÚK Dobrovského – Svitavská radiála SO 203" (Brno city, Dobrovskeho - Svitavska crossroads. Pile load test - final report), VUIS, Bratislava, Slovakia, Rep. 54/2009, 2010. (in Slovak)

[30] Homaifar, A., Qi, C. X., Lai, S. H. "Constrained Optimization Via Genetic Algorithms", Simulation, 62(4), pp. 242–253, 1994. https://doi.org/10.1177/003754979406200405